GEOPHYSICS, VOL. 62, NO. 3 (MAY-JUNE 1997); P. 775–785, 8 FIGS., 1 TABLE.

Straightforward inversion of vertical electrical sounding data

Pravin K. Gupta*, Sri Niwas*, and Vinod K. Gaur‡

ABSTRACT

A straightforward inversion scheme (SIS) has been developed to interpret vertical electrical sounding data. This scheme does not require quasi-linearization of the inverse resistivity problem and thereby dispenses with the iterative process and the necessity of guessing the number of layers and their resistivities and thicknesses. The entire solution domain is divided into uniform thickness layers, whose scale must be judiciously selected for the desired resolution. The apparent resistivity formula can now be posed as an underdetermined matrix equation whose minimum norm solution is downward continued to obtain the reflection coefficients which, in turn, yield the vertical resistivity distribution. A recurrence relation has been developed especially for this purpose. In general, when data are expected to be noisy, a regressed minimum norm solution is used. Exhaustive tests of the algorithm have established its numerical efficiency. Results of six typical synthetic models, representing diverse geological conditions, as well as results of two field examples are included to demonstrate this claim.

INTRODUCTION

The wide ranging applicability of vertical electrical sounding methods to resource exploration and engineering investigations continues to spur the search for even better techniques for the interpretation of resistivity data. The starting point for all such endeavours remains Stefanescu's (1930) expression which describes, in terms of the thicknesses and resistivities of various layers, the potential around a point current electrode grounded at the surface. Langer (1933) showed that if the ground resistivity continuously varies with depth and the potential distribution about a current electrode grounded at the surface is completely known, then the inverse potential problem has a unique solution. Subsequently, Slichter (1933) showed how apparent resistivity values, computed from surface potential data, could be used to estimate the resistivity kernel function from which the layer parameters could be inferred. This he called the "direct" method and its several variants (Pekeris, 1940; Vozoff, 1958; Koefoed, 1970, 1979; Ghosh, 1971a) emerged in efforts to improve its effectiveness. The large number of computations involved in these techniques and their inherent complexity, however, greatly restricted their applications. Meanwhile, parallel developments in the use of indirect methods (Flathe, 1955; Onodera, 1960; Roman, 1963; Van Dam, 1964; Mooney et al., 1966; Ghosh, 1971b) based on the availability of a large number of master curves derived from forward solutions, became dominant despite their poorer resolving capability. Later, with the availability of fast computers, resistivity interpretation was revolutionized by quasi-linearizing the essentially nonlinear inverse resistivity problem and using various linear inversion schemes (Inman et al., 1973; Inman, 1975; Bichara and Lakshmanan, 1976; Jupp and Vozoff, 1975; Johansen,1977 and Constable et al., 1987).

The quasi-linear inversion method requires an educated guess of resistivity variation fairly close to the real situation. This requirement always proved to be a serious disadvantage. Furthermore, the iterative nature of the algorithm made it necessary, for each iteration, to first solve the forward problem and then invert the system matrix for the correction vector . In the absence of any a priori knowledge, a liberally overparameterized initial guess model just did not succeed (Inman et al., 1973; Wu, 1968) and a thin layer problem had little chance of being resolved adequately.

In this paper we present a noniterative straightforward inversion scheme (SIS) for interpreting vertical electrical sounding (VES) data. The method does not require an initial guess of layer resistivities and thicknesses, all it asks for is a layer thickness unit parameter that must be judiciously chosen keeping in mind the resolution desired. The method provides a near-continuous vertical resistivity distribution. The algorithm has been tested extensively using interesting synthetic models and real field data, and eight of these exercises are presented here. Of these, the three models of Gai-Shan (1985) and the model of Parker (1984) are of special interest, as these models could not be inverted satisfactorily by these authors. The SIS algorithm inverted these models successfully, thereby establishing its effectiveness.

Manuscript received by the Editor March 18, 1994; revised manuscript received September 5, 1996.
*Department of Earth Sciences, University of Roorkee, Roorkee, India 247 667.
‡CSIR Centre for Mathematical Modeling and Computer Simulation at National Aerospace Laboratories, Bangalore, India 560 037.

FORMULATION OF THE ALGORITHM

Stefanescu (1930) derived the electrical potential $U(s)$ on the surface ($z = 0$) of a layered earth at a distance s from a grounded electrode carrying a current I, as

$$U(s) = \frac{I}{2\pi}\int_0^\infty T_1(\lambda)J_0(\lambda s)\,d\lambda, \tag{1}$$

where $J_0(\lambda s)$ is the zeroeth order Bessel function of the first kind, $T_1(\lambda)$ is the electrical impedance at the surface, defined in Koefoed (1970) as the resistivity transform function of layer resistivities and thicknesses, and λ is the integration variable. Koefoed (1979) also disassociated the resistivity transform function to extract the resistivity kernel function $K_1(\lambda)$ representing the deviations in response of the layered earth from that of a homogeneous half-space. Accordingly, at the air-earth interface

$$T_1(\lambda) = \rho_1[1 + 2K_1(\lambda)], \tag{2}$$

while at the top of the ith layer,

$$T_i(\lambda) = \rho_i[1 + 2K_i(\lambda)]. \tag{3}$$

From these basic expressions, Sri Niwas and Israil (1986, 1987) obtained the following simple expression for the apparent resistivity, $\rho_a(s)$, measured by a symmetrical four electrode array

$$\rho_a(s) = \sum_{j=0}^{\infty} T_{1j}G_j^{(2)}(s), \tag{4}$$

where

$$G_j^{(2)}(s) = \frac{m}{m-1}G_j^{(1)}(s) - \frac{1}{m-1}G_j^{(1)}(ms). \tag{5}$$

Here,

$$G_j^{(1)}(s) = \frac{s}{\left(\epsilon_j^2 + s^2\right)^{1/2}}, \tag{6}$$

which is the Green's function of a point source, ϵ_j being a real constant. The parameter m in equation (5) defines specific electrode configurations, e.g., Wenner ($m = 2$), Schlumberger ($1 < m < 1.1$), pole-pole ($m = \infty$).

Expression (4) was obtained by writing, $T_1(\lambda)$, corresponding to the air-earth interface, in the form of a series

$$T_1(\lambda) = \sum_{j=0}^{\infty} T_{1j}\epsilon^{-\epsilon_j\lambda}, \qquad \epsilon_0 = 0, \tag{7}$$

and then using the Lipschitz integral (Watson, 1966). The set of ϵ_j in equations (6) and (7) were selectively identified to minimize the number of series terms required for an acceptable representation. For the apparent resistivity values $\rho_a(s_\ell)$, determined for n different electrode spacings s_ℓ, equation (4) can be written in a matrix form as

$$\mathbf{v} = \underset{\sim}{\mathbf{G}}\mathbf{f}, \tag{8}$$

where

$$\mathbf{v} = [\rho_a(s_1), \rho_a(s_2), \ldots, \rho_a(s_n)]^t,$$

$$\mathbf{f} = [T_{11}, T_{12}, \ldots, T_{1p}]^t,$$

and

$$G_{1j} = G_j^{(2)}(s_i).$$

Here, superscript t denotes matrix transpose operation.

The minimum norm solution $\hat{\mathbf{f}}$ obtained from equation (8) is given by

$$\hat{\mathbf{f}} = \underset{\sim}{\mathbf{G}}^t - (\underset{\sim}{\mathbf{G}}\underset{\sim}{\mathbf{G}}^t)^{-1}\mathbf{v}. \tag{9}$$

Equation (8) offered an efficient algorithm for transforming apparent resistivity data to resistivity transform data and vice-versa. However, it did not lead to any significant advance in methodology for the inference of subsurface resistivity distribution. The basic reason for this results from the fact that ϵ_j was assigned fixed values independent of model structure. This, in turn, led to the coefficients T_{1j} being implicit functions of both layer thicknesses and resistivities.

Equation (7) reveals that for a model of uniform layer thickness (d), the choice of $\epsilon_j = 2jd$ would make T_{1j} a function of layer resistivities alone. Furthermore, in equation (4), the apparent resistivity values can be interpreted as superposed contributions from a number of sources (images), each of strength T_{1j} with G_j, with the corresponding Green's functions as weights. Thus, the deviatoric potentials measured at the surface are seen as the sum of individual influences arising from different layers.

The possibility of decomposing the apparent resistivity into components that can be identified with specific layers provides the basic motivation for designing an algorithm that would invert apparent resistivity data directly in terms of the layer resistivities of a stratified earth.

To accomplish this, we first define a layered earth model resting on a semi-infinite substratum (Figure 1). Each layer in this

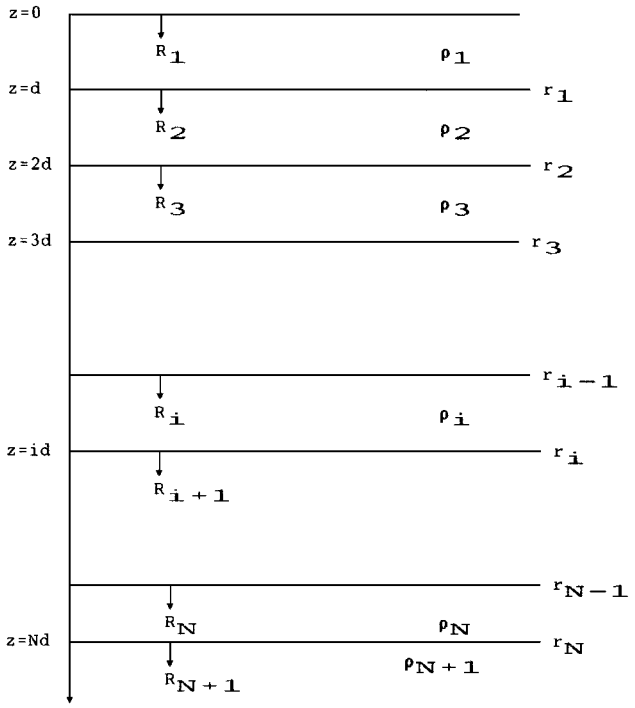

FIG. 1. Geometry of uniformly thick N-layered earth.

model has the same thickness, judiciously selected to ensure that the thinnest resolvable layer is characterized distinctly. The geoelectric section of this model can then be described completely by layer resistivities (ρ_i) alone.

The reflection coefficient r_i of the ith layer with respect to the $(i+1)$th layer, is given by

$$r_i = \frac{\rho_{i+1} - \rho_i}{\rho_{i+1} + \rho_i}. \tag{10}$$

The reflection function R_i is related to the resistivity transform function $T_i(\lambda)$ by the following relations (Aassal and Mahmoud, 1987).

$$T_i(u)\big|_{Top} = \rho_i \frac{1 + R_i(u)}{1 - R_i(u)} \tag{11}$$

and

$$T_i(u)\big|_{Bottom} = \rho_{i-1} \frac{1 + R_{i-1}(u)/u}{1 - R_{i-1}(u)/u}, \tag{12}$$

where

$$u = e^{-2\lambda d}.$$

The equality of equations (11) and (12) for $T_i(u)$ ensures continuity of the electrical impedance through the layer and yields the following recurrence relation for R_i,

$$R_{i-1}(u) = \frac{R_i(u) + r_{i-1}}{1 + R_i(u) r_{i-1}} u \tag{13}$$

with

$$R_{N+1}(u) = 0.$$

It may be noted that $|r_i| < 1$ for all finite nonzero values of layer resistivities, $R_i(u) < 1$ for all i and $u < 1$ for all positive values of d. Therefore, the denominator in equation (13) can be expanded in a binomial series and $R_i(u)$ can be expressed, for all i, as the polynomial in u given below as

$$R_i(u) = \sum_{j=1}^{\infty} R_{ij} u^j. \tag{14}$$

Using this expansion in equation (13) and equating the coefficients of equal powers of u, we obtain the following forward recurrence relation,

$$\begin{aligned} R_{i-1,j} &= r^*_{i-1} R_{i,j-1} + R^*_{i1} R_{i-1,j-1} \\ &\quad + R^*_{i2} R_{i-1,j-2} + \cdots + R^*_{i,j-2} R_{i-1,2}, \end{aligned} \tag{15}$$

where,

$$r^*_{i-1} = \left(1 - r^2_{i-1}\right), \qquad R^*_{ij} = -r_{\ell-1} R_{ij}.$$

Similarly, the expression for $T_i(u)$ at the top of the ith layer can be written as a polynomial

$$T_i(u) = \sum_{j=0}^{\infty} T_{ij} u^j. \tag{16}$$

Here $T_{i0} = \rho_i$ and for $j > 0$, the coefficients are related to R_{ij}, as

$$\begin{aligned} T_{ij} &= T_{i0} R_{ij} + R_{i,j-1} T_{i,1} + R_{i,j-2} T_{i,2} + \cdots \\ &\quad + R_{i,2} T_{i,j-2} + R_{i1} T_{i,j-1}. \end{aligned} \tag{17}$$

Rewriting equation (9) as

$$\hat{\mathbf{f}} = \underset{\sim}{\mathbf{G}}^t \mathbf{w}$$

with

$$\mathbf{w} = (\underset{\sim}{\mathbf{G}}\underset{\sim}{\mathbf{G}}^t)^{-1} \mathbf{v},$$

T_{1j}, the jth component of vector $\hat{\mathbf{f}}$, can be expressed as

$$T_{1j} = \sum_{\ell} \mathbf{G}_{j\ell} w_\ell, \qquad j \geq 0. \tag{18}$$

Therefore, as $G_{01} = 1$ for all ℓ,

$$\rho_1 = T_{10} = \sum_{\ell=1}^{n} w_\ell.$$

Using equation (17), the coefficient R_{1j} can be related to T_{1j} as

$$\begin{aligned} 2\rho_1 R_{1j} &= T_{1j} - T_{1,j-1} R_{11} - T_{1,j-2} R_{12} - \cdots \\ &\quad - T_{12} R_{1,j-2} - T_{11} R_{1,j-1}. \end{aligned} \tag{19}$$

In turn, using equation (15), the following inverse recurrence relation can be written as

$$\begin{aligned} R_{ij} = \frac{1}{r^*_{i-1}} \big[& R_{i-1,j+1} - R_{i-1,j} R^*_{i1} - R_{i-1,j-1} R^*_{i2} - \cdots \\ & - R_{i-1,3} R^*_{i,j-2} - R_{i-1,2} R^*_{i,j-3} \big], \end{aligned} \tag{20}$$

Finally, we obtain the various reflection coefficients and layer resistivities as

$$r_i = R_{i1}$$

and

$$\rho_{i+1} = \frac{1 + R_{i1}}{1 - R_{i1}} \rho_i. \tag{21}$$

Equations (18) through (21) provide a complete solution of the inverse resistivity problem.

Numerical consideration

An algorithm was developed accordingly to apply this straightforward inversion scheme (SIS) to extract subsurface resistivities from observed values of apparent resistivities. This algorithm comprises two stages. In the first stage, the minimum norm solution vector $\hat{\mathbf{f}}$ is obtained, while in the second stage, this solution is used to retrieve the resistivity distribution by downward continuation. The quality of inversion is monitored after both these stages by recomputing the response vector. It may be added here that the algorithm has the capacity to handle a very large number of terms in the exponential series representation. It would, in practice, be restricted to a reasonable number "p", depending upon the desired accuracy "e_0," given by $p = 0.5 s_{\max}/(d\sqrt{e_0})$ with $s_{\max}$ being the maximum electrode spacing.

The estimated solution vector $\hat{\mathbf{f}}$ in equation (9) is used to assess the quality of the inverse solution by first computing the response vector $\hat{\mathbf{v}}$ as

$$\hat{\mathbf{v}} = \underset{\sim}{\mathbf{G}} \hat{\mathbf{f}} \tag{22}$$

and then computing the error parameter e_r as the relative root-mean-square (rms) error between $\mathbf{v}$ and $\hat{\mathbf{v}}$ as

$$e_r^2 = \sum_{i=1}^{n} \frac{[(v_i - \hat{v}_i)/v_i]^2}{n}, \tag{23}$$

where n is the number of data points. Note that equation (9) will yield results only when equation (8) is consistent and full rank. However, in the case of field data, as well as in case of random noise-added synthetic data, the consistency is nonexistent. In such cases the solution is achieved through a regularized minimum norm estimator and is given by

$$\hat{\mathbf{f}} = \underset{\sim}{\mathbf{G}}^t(\underset{\sim}{\mathbf{G}}\underset{\sim}{\mathbf{G}}^t + \underset{\sim}{\mathbf{E}})^{-1}\mathbf{v}, \tag{24}$$

where $\underset{\sim}{\mathbf{E}}$ is the data error covariance matrix. If this matrix is not available, it can be approximated as $e^2\underset{\sim}{\mathbf{I}}$ with e being the average noise to signal ratio.

To estimate the quality of inverted conductivity model, the misfit ϵ_t between its computed response $\mathbf{v}$ and the observation $\mathbf{v}$ can be computed in a manner similar to that used for ϵ_r as

$$\epsilon_t^2 = \sum_{i=1}^{n} \frac{[(v_i - v_i)/v_i]^2}{n}.$$

The vector $\hat{\mathbf{f}}$, given by either equation (9) or (24), can be viewed as the initial condition of an initial value problem, which means that as the solution is continued downward, the error in $\hat{\mathbf{f}}$ will propagate and may become enhanced. This error propagation may sometimes lead to nonphysical reflection coefficients lying outside the $(-1, 1)$ interval. This should always be taken as a warning sign, that no further downward continuation of conductivity profile is possible. Such eventuality will occur only if the regression parameter is not able to account for the error in data and/or the 1-D model is incompatible with the real conductivity distribution. A possible way out is to use a higher regression parameter value. The higher regression parameter value will lead to the increased misfit and blurred conductivity profile. Further, for the smooth functioning of SIS algorithm, the inverted reflection coefficients should be approximated as zero whenever it lies within a prescribed infinitesimal interval. In the present study this interval is $-.01$ to .01. It may be alluded here that ϵ_t will, in general, be greater than ϵ_r because the former depends on the final outcome of the initial value problem, while the latter is derived only from the initial conditions represented by vector $\hat{\mathbf{f}}$.

TESTS OF THE SIS ALGORITHM

This algorithm was subjected to rigorous tests by using it to invert a large variety of layered earth models. In particular, the effects of overparameterization, or very fine layering, and of measurement errors were studied to appraise the quality of resulting inverse solutions. It may be alluded here that all the models were run on an IBM compatible PC-486 with 32 MB RAM. The computer time required for the various models varied from 1.8 s to 10.4 s.

The test results of eight models presented below represent a broad range of subsurface conditions encountered in nature. Six of these use forward synthesized solutions as data inputs for inverting the model. Models I, II, and III are the theoretical geoelectric sections used in Gai-Shan (1985). Model IV is taken from Parker (1984). Model V is the geological model of Inman et al. (1973) and model VI is constructed from borehole and well log data. Of the two field data sets inverted, one is from a shallow section for which drill data was available for comparison and the other is from a deeper section. Note that the Wenner response was generated for model IV while the Schlumberger response was computed for all the remaining synthetic models. In all cases, the layer thickness unit (d) was taken to be 2 m, while the electrode spacing ranged from 1 m to a maximum value depending upon the depth of the investigation (Roy and Apparao, 1971). There were ten spacing values in a decade.

Theoretical models—Synthesized data

The first three models were taken from Gai-Shan (1985), who interpreted these in terms of composite parameters: total longitudinal conductance, total transverse resistance, and the substratum resistivity. This strategy was dictated by the difficulty in obtaining a quasi-linearized iterative solution in terms of layer parameters. Using the SIS, however, we were able to obtain the vertical resistivity variations by overparameterizing the Gai-Shan models, which are:

$$\begin{aligned}
\text{Model I}: &\ \rho_1 = 20 \text{ ohm-m}, d_1 = 20 \text{ m}; \rho_2 = 10 \text{ ohm-m},\\
&\ d_2 = 20 \text{ m}; \rho_3 = 1 \text{ ohm-m}\\
\text{Model II}: &\ \rho_1 = 10 \text{ ohm-m}, d_1 = 20 \text{ m}; \rho_2 = 2 \text{ ohm-m},\\
&\ d_2 = 20 \text{ m}; \rho_3 = 5 \text{ ohm-m}, d_3 = 50 \text{ m};\\
&\ \rho_4 = 2 \text{ ohm-m}, d_4 = 20 \text{ m}; \rho_5 = 100 \text{ ohm-m}\\
\text{Model III}: &\ \rho_1 = 1 \text{ ohm-m}, d_1 = 2 \text{ m}; \rho_2 = 2 \text{ ohm-m},\\
&\ d_2 = 4 \text{ m}; \rho_3 = 3 \text{ ohm-m}, d_3 = 6 \text{ m};\\
&\ \rho_4 = 4 \text{ ohm-m}, d_4 = 8 \text{ m}; \rho_5 = 5 \text{ ohm-m},\\
&\ d_5 = 10 \text{ m}; \rho_6 = 6 \text{ ohm-m}, d_6 = 12 \text{ m};\\
&\ \rho_7 = 30 \text{ ohm-m}.
\end{aligned}$$

Model II was studied twice using different half-space resistivity values 100 ohm-m [model II(a)] and 1 ohm-m [model II(b)]. Schlumberger apparent resistivity values were computed for the three models, using maximum spacing values of 500, 1200, and 500 m, respectively.

The apparent resistivity curves along with the corresponding true and inverted models are presented in Figure 2. It is evident that none of the apparent resistivity curves yields information about the correct number of layers in the true model. As a result, any quasi-linear inversion algorithm, needing an initial guess model, would not succeed as confirmed by the experience of Gai-Shan (1985). SIS, however, in all the four cases yielded inverted models close to the true models. The number of 2 m thick layers, in the four cases were 25, 70, 70, and 30. The quality of inverted models versus true models is quite good as shown in Figure 2 and evidenced by the values of relative rms error e_r which were 2.86×10^{-8}, 4.55×10^{-8}, 7.85×10^{-8}, and 9.31×10^{-10}, respectively. Note that in the case of Model II(a), the SIS is able to decipher the highly conducting (2 ohm-m), 20 m thick layer at a depth of 90 m.

Model III is difficult to invert as the interlayer resistivity variations are quite small (1 ohm-m). Yet the 30-layer model ($d = 2$ m) retrieves the original model parameters rather well.

The inverted models in Figure 2 reveal that even though the true half-space resistivity values are not attained, the half-space conductive/resistive nature is retrieved. In these cases the half-space resistivity values can always be estimated from asymptotic values of apparent resistivity for the larger electrode spacings.

Model IV, having following continuous resistivity variation was introduced in Parker (1984) and was also studied by Simms and Morgan (1992),

$$\rho(z) = 500(1 + 0.2z)^{-2}.$$

This variation is shown in Figure 3 as the curve mod0. The two inverted models of Parker (1984), with layer thicknesses 2 m (imod02) and 14 m (imod14), are reproduced in Figure 3a. The four inverted models obtained by Simms and Morgan (1992), using variable parameters (imodv) and uniform (imodu), geometric progression (imodg) and logarithmic progression (imodl) layer thicknesses, are given in Figure 3b. Clearly, the inverted models of both these studies are unsatisfactory. A detailed study of this resistivity variation was therefore carried out using the SIS algorithm, and the results are plotted in Figure 3c.

For this purpose, the ten data values, given in Parker (1984) and listed in Table 1, were used to invert for the 50-layer model with a layer thickness unit of $d = 2$ m. The corresponding

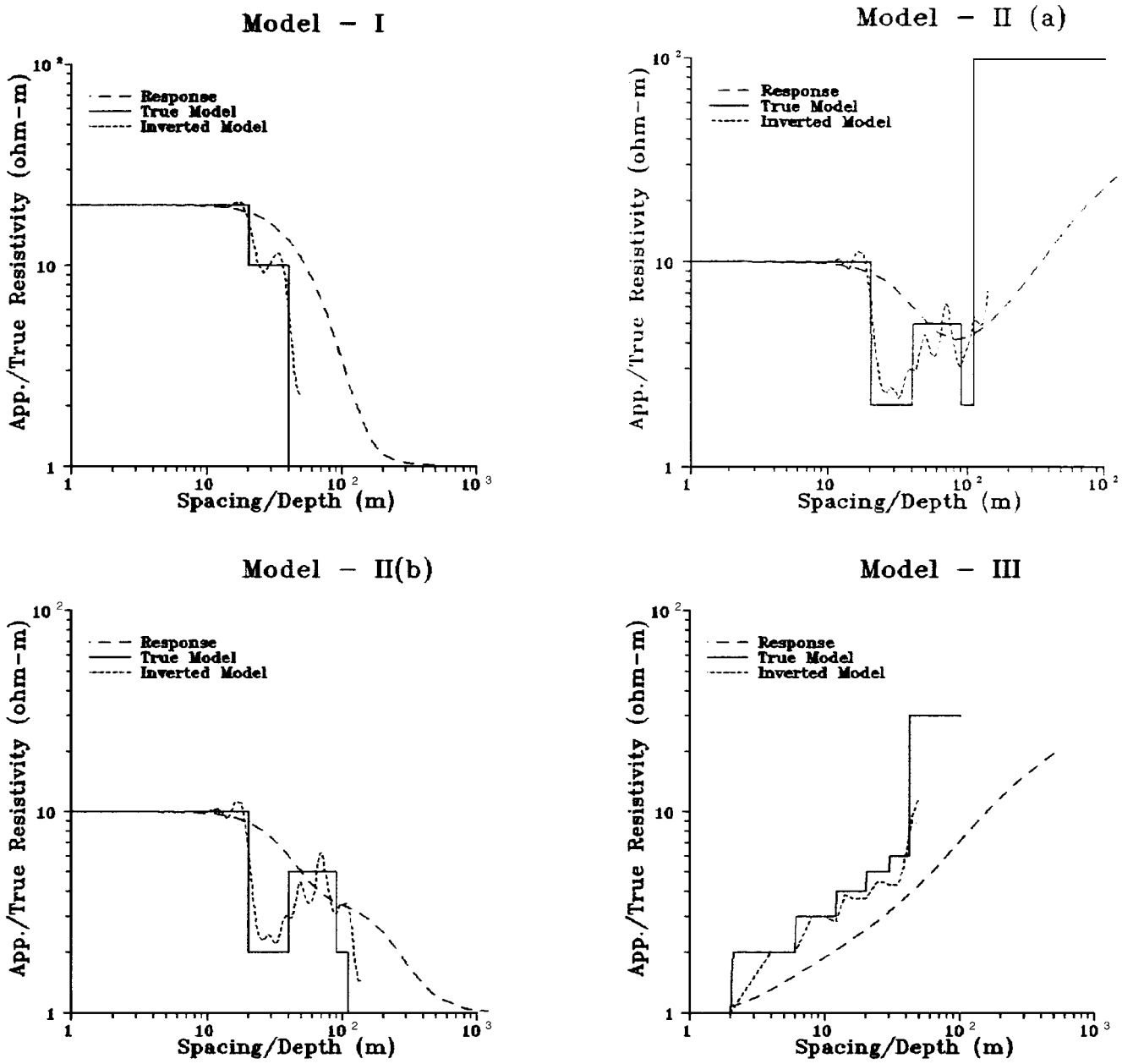

FIG. 2. Inversion of resistivity responses of models I, IIa, IIb, and III.

inverted model is shown as curve imod1. This solution is unstable suggesting that the data may be erroneous. This fact was confirmed when the SIS algorithm was rerun with regression parameter $e = 0.001$. The resulting smooth model is shown as curve imod2. To evaluate the quality of inverted model imod2, the SIS algorithm was used to generate Wenner synthetic data for the same ten electrode spacing values. These response values are also listed in Table 1. The inversion of this data set without regression yielded the curve imod3 that is not only smooth but slightly better than imod2. This suggests once again that the oscillations in imod1 were mainly a result of erroneous data. Last, a larger data set for 25 spacing values was generated and used to obtain the inverted model imod4, which is significantly closer to true model mod0 in comparison to imod2 and imod3. A comprehensive study of Figure 3 illustrates the higher quality of the SIS solutions in comparison to the solutions in Parker (1984) and Simms and Morgan (1992).

Note that the e_r values for imod1, imod2, imod3, and imod4 were 2.34×10^{-11} , 1.58×10^{-3}, 5.58×10^{-13}, and 1.87×10^{-9}, respectively. The error in case of imod2 is of the order of regression parameter chosen.

Geological model—Synthesized data

We studied two models constructed from a geological section for which both drill and well log data were available. Model V (Figure 4) is a geologically inspired model taken from Inman et al. (1973), while model VI (Figure 5) represents subsurface

Table 1. Wenner apparent resistivity values at the ten points used for obtaining SIS solutions imod1, imod2, and imod3.

Electrode separation (m)	Apparent resistivity (Ohm-m)	
	Parker (1984)	SIS
1.0	486.5	479.3
2.0	473.7	472.0
5.0	438.7	439.1
10.0	389.5	389.8
20.0	314.4	314.8
50.0	186.0	188.2
100.0	96.22	106.7
150.0	57.90	78.7
200.0	38.26	67.7
250.0	26.97	63.0

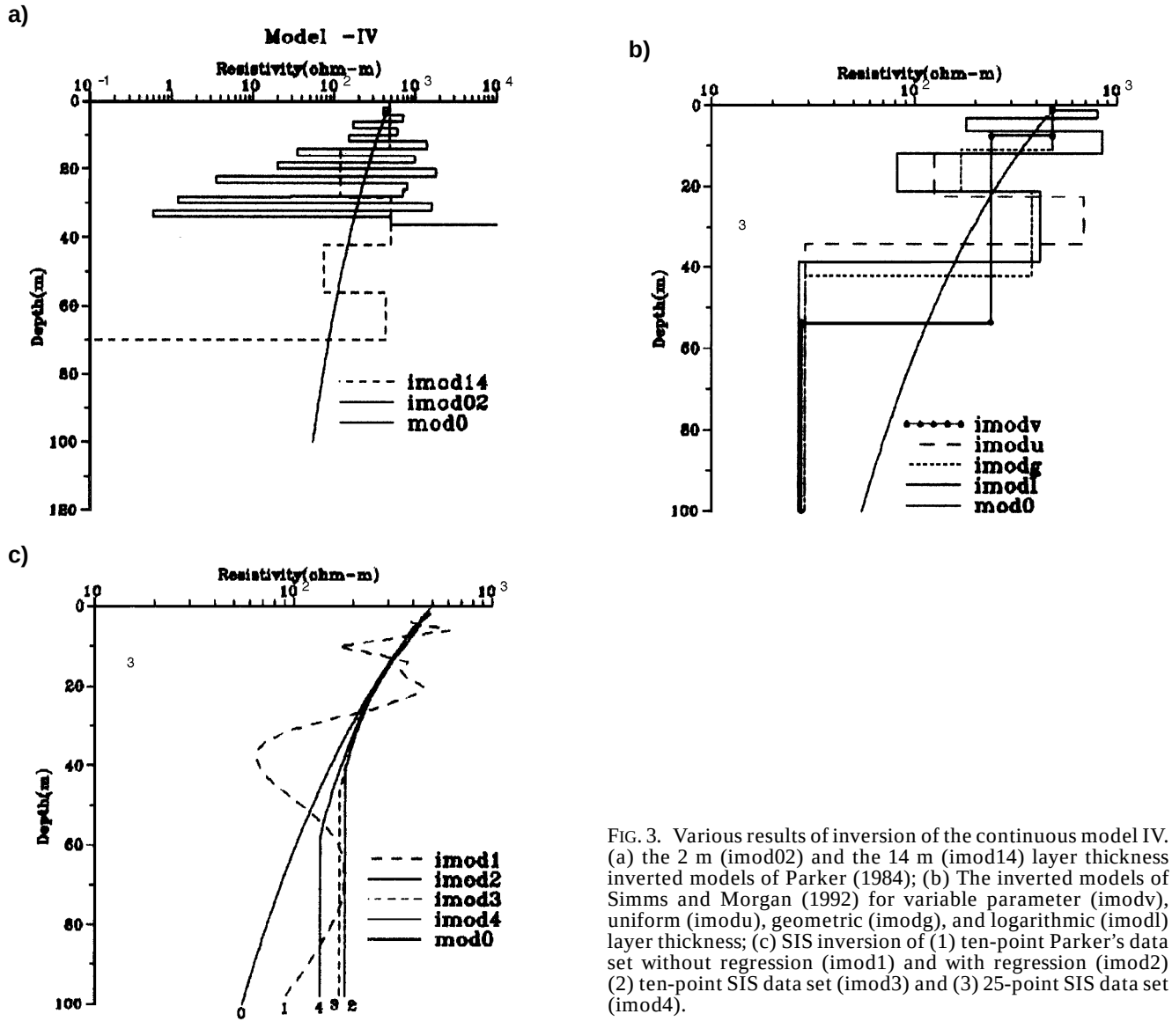

FIG. 3. Various results of inversion of the continuous model IV. (a) the 2 m (imod02) and the 14 m (imod14) layer thickness inverted models of Parker (1984); (b) The inverted models of Simms and Morgan (1992) for variable parameter (imodv), uniform (imodu), geometric (imodg), and logarithmic (imodl) layer thickness; (c) SIS inversion of (1) ten-point Parker's data set without regression (imod1) and with regression (imod2) (2) ten-point SIS data set (imod3) and (3) 25-point SIS data set (imod4).

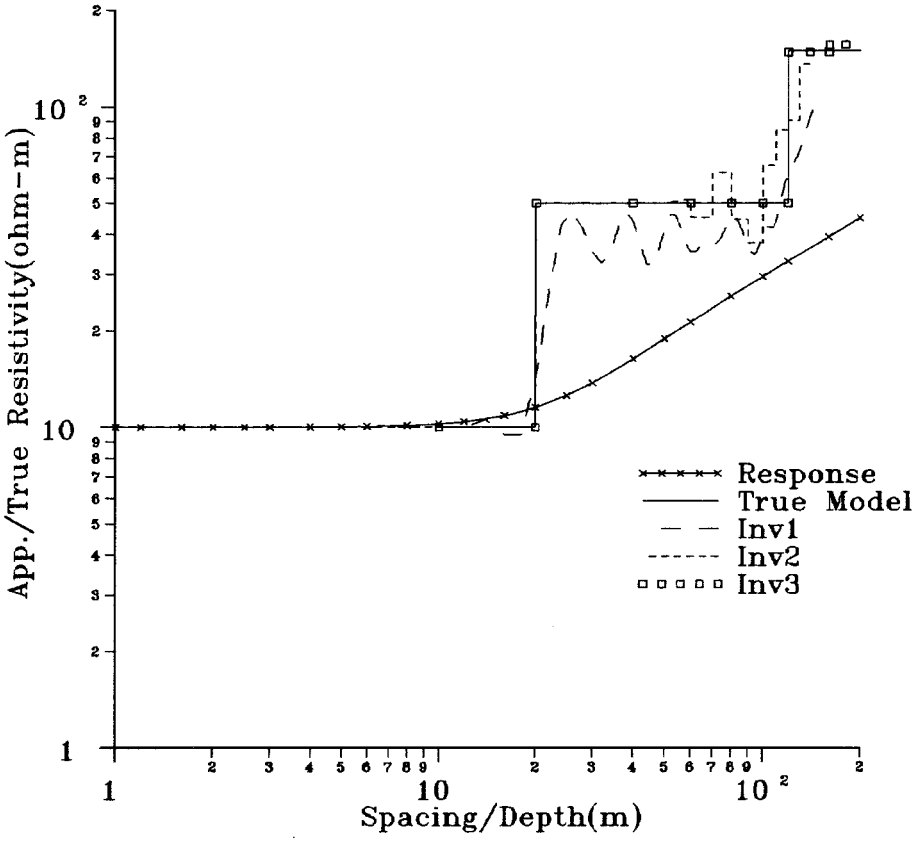

FIG. 4. The apparent resistivity response, the true model and the inverted models for model V (from Inman et al. 1973) with layer thickness unit $d = 2$ m (Inv1), 10 m (Inv2), and 20 m (Inv3).

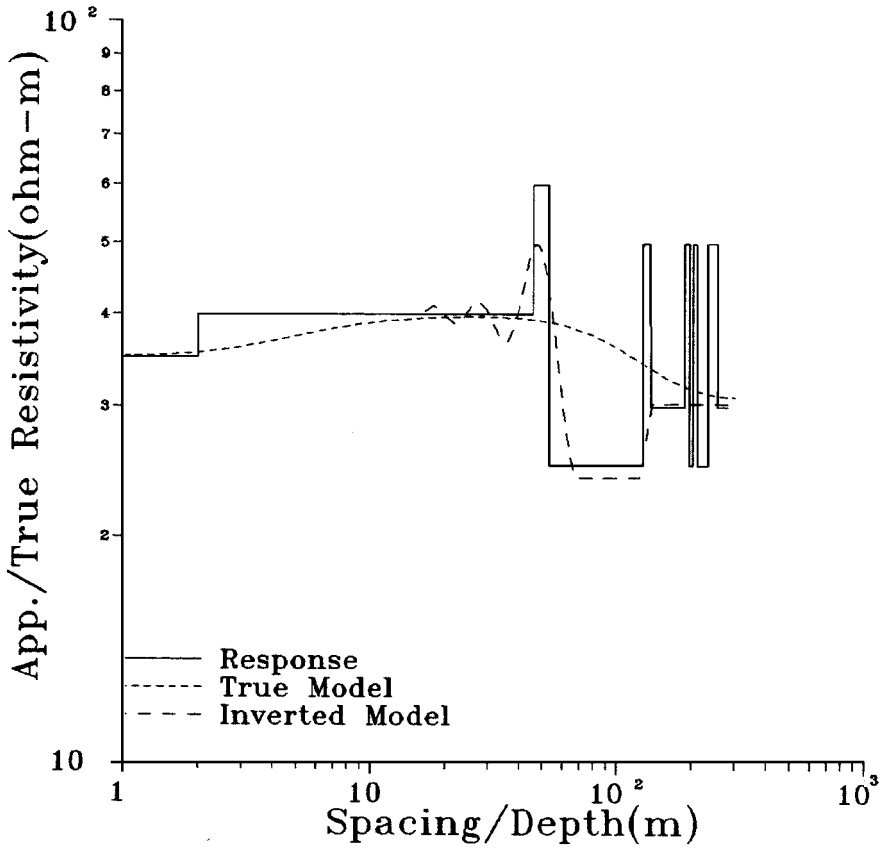

FIG. 5. The apparent resistivity inversion model for model VI constructed from borehole and well log data at a site near Delhi.

conditions comprising alternate layers of clay and clay enriched sands. The parameters of these two models are:

Model V : $\rho_1 = 10$ ohm-m, $d_1 = 20$ m (wet soil);
$\rho_2 = 50$ ohm-m,
$d_2 = 100$ m (clay and gravel);
$\rho_3 = 150$ ohm-m (bed rock)

Model VI : $\rho_1 = 35$ ohm-m, $d_1 = 2$ m; $\rho_2 = 40$ ohm-m,
$d_2 = 43.5$ m; $\rho_3 = 60$ ohm-m, $d_3 = 7.5$ m;
$\rho_4 = 25$ ohm-m, $d_4 = 75$ m; $\rho_5 = 50$ ohm-m,
$d_5 = 9$ m; $\rho_6 = 30$ ohm-m, $d_6 = 50$ m;
$\rho_7 = 50$ ohm-m, $d_7 = 9$ m; $\rho_8 = 25$ ohm-m,
$d_8 = 7.5$ m; $\rho_9 = 50$ ohm-m, $d_9 = 7$ m;
$\rho_{10} = 25$ ohm-m, $d_{10} = 23$ m;
$\rho_{11} = 50$ ohm-m, $d_{11} = 22$ m;
$\rho_{12} = 30$ ohm-m.

Model V was studied by Inman et al. (1973) using the generalized linear inverse. The authors were, however, unable to obtain a reasonable solution unless the initial guess for the starting model was very close to the true one.

Synthesized Schlumberger apparent resistivity data for model V was inverted using the SIS algorithm for three different scales of parameterization: 75 layers ($d = 2$ m), 15 layers ($d = 10$ m) and 10 layers ($d = 20$ m). The corresponding inverted models are shown in Figure 4 as curves inv1, inv2, and inv3. The relative rms errors e_r in these three cases were 2.81×10^{-9}, 6.05×10^{-9}, and 1.18×10^{-9}, respectively. The corresponding ϵ_t values were 0.075, 0.030, and 0.032, respectively. With the finest layering, the SIS solution retrieves the first two layers accurately as being, respectively, 10-unit and 50-unit thick, with their resistivity values mildly oscillating about a mean value close to the true one. The third layer resistivity value is approached asymptotically.

The 15-layer SIS solution is of excellent quality, recovering the first layer and half of the second layer exactly and the remaining ones reasonably close. Encouraged by this improvement, a third SIS solution was sought in which the unit thickness was set equal to that of the top layer. As shown in Figure 4, this ten layer ($d = 20$ m) inversion faithfully reproduces the true model. This exercise highlights two important characteristics of SIS. First is the effect of overparameterization in the form of spurious oscillations in the inverted resistivity values, centered around the true layer resistivity values. Second, an appropriate choice of the unit thickness enables accurate retrieval of layer resistivities and thicknesses even in case of models with high-resistivity contrasts.

For model VI, the apparent resistivity profile, the true model and the inverted model are given in Figure 5. It is evident that the apparent resistivity profile is blind to the pattern of subsurface layering, the 150-layer ($d = 2$ m) SIS inversion is able to retrieve model resistivity values rather closely to a depth of 187 m. Below this depth the various layers merge indicating that the vertical resistivity sounding method cannot resolve the thin layers at depths greater than 200 m. The rms error values ϵ_r and ϵ_t were 2.01×10^{-8} and 0.03, respectively.

Inversion of noisy data

The robustness of the SIS algorithm was evaluated by studying the effect of random noise on the quality of inverted solutions. We obtained the inverted solutions of model V with $d = 20$ m when the synthesized data is corrupted with random Gaussian noise in the proportions 0.5, 1, 2, 5, 10, and 20%. The respective relative rms error ϵ_r values in these cases were 0.00001, 0.00874, 0.0116, 0.0463, 0.0966, and 0.22. The corresponding ϵ_t values were 0.034, 0.015, 0.024, 0.050, 0.120, and 0.226, respectively. The resulting SIS solutions for 0, 5, 10, and 20% cases are shown in Figure 6. It was observed that up to a 2% noise level the inverted models were very close to the no error case. Figure 6 reveals that while the presence of noise does cause a blurring of the solution sharpness, a reasonably fair solution is obtained even at a 20% level, thereby establishing the robustness of the SIS algorithm.

Straightforward inversion of field data

The remarkable power of SIS illustrated by the quality of inverted solutions, led us to apply it extensively to the interpretation of actual field data. Two cases discussed here refer to shallow and deep exploration. Apparent resistivity data for field model I were obtained from electrical sounding at a site in the village Aurangabad of Haridwar District in the Shiwalik range of outer Himalaya in Uttar-Pradesh. The drill record was available to a depth of 131 m. Two 40 layer SIS solutions for $d = 5$ m are plotted as curves inv2 and inv5 in Figure 7 along with the drill data and ρ_a values. The regression parameter values for the two inversions were equal to 0.02 and 0.05. The rms error ϵ_r in two cases were 0.121 and 0.134, while the ϵ_t values were 0.277 and 0.180, respectively. Both the SIS solutions are in good agreement with the lithology recorded during drilling, especially the sand pebbles (aquifer) at a drill depth of 35 m.

Field data II, taken from Singh et al. (1988), was recorded at a site in the Saurashtra region, Western India, where the general stratigraphy from top to bottom is: thin soil cover, moderately conducting basaltic (trap) layer, thick resistive layer of compact basalt, conducting porous sediments, and highly resistive basement layer.

Since the electrical sounding curve for this area is rather long, we first obtained a 50-layer ($d = 100$ m) SIS solution, and then used the left-hand ascending part of the curve to obtain a 100-layer ($d = 2$ m) SIS solution for the shallower section, with the regression parameter used being 0.05 in both cases. The rms error ϵ_r in these two cases were 0.072 and 0.033, while the ϵ_t values were 0.308 and 0.194, respectively. The two solutions were appended to obtain the composite SIS solution plotted in Figure 7 along with the apparent resistivity curve and the inferred geological section.

The SIS solution appears to be the best possible that can be retrieved from field data. Its robust character is further enhanced by the possibility of constructing composite SIS solutions from resistivity sounding data obtained by intelligently segmenting the sounding curve in a way that would substantially isolate the responses arising from different depth ranges.

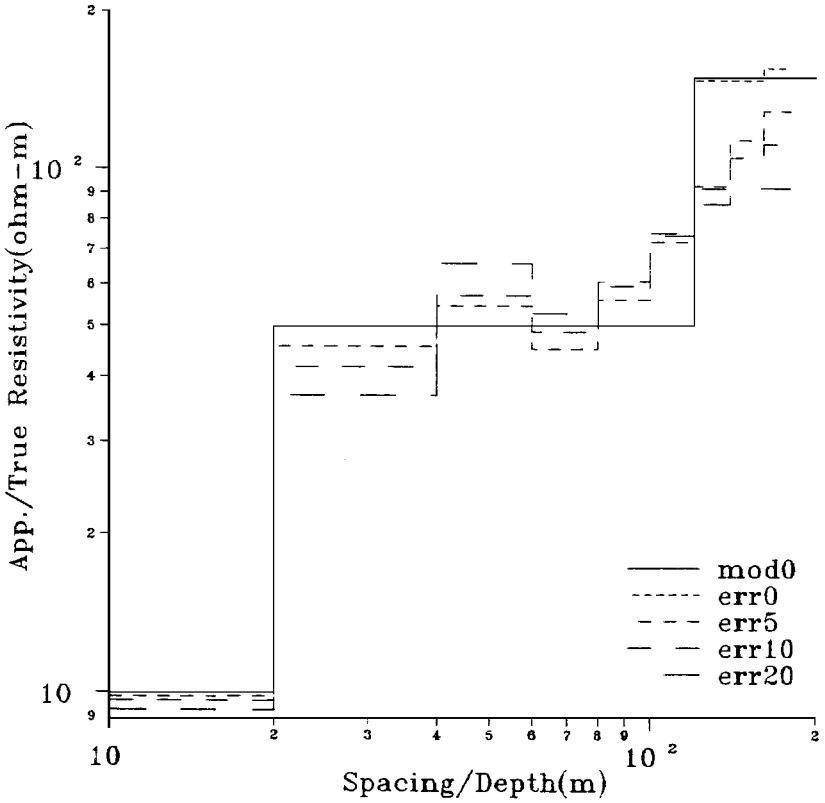

FIG. 6. Effect of random Gaussian noise in apparent resistivity data for model V with $d = 20$ m case. The true model (imod0) and the inverted models for the error-free (err0), 5% (err5), 10% (err10), and 20% (err20) noise levels.

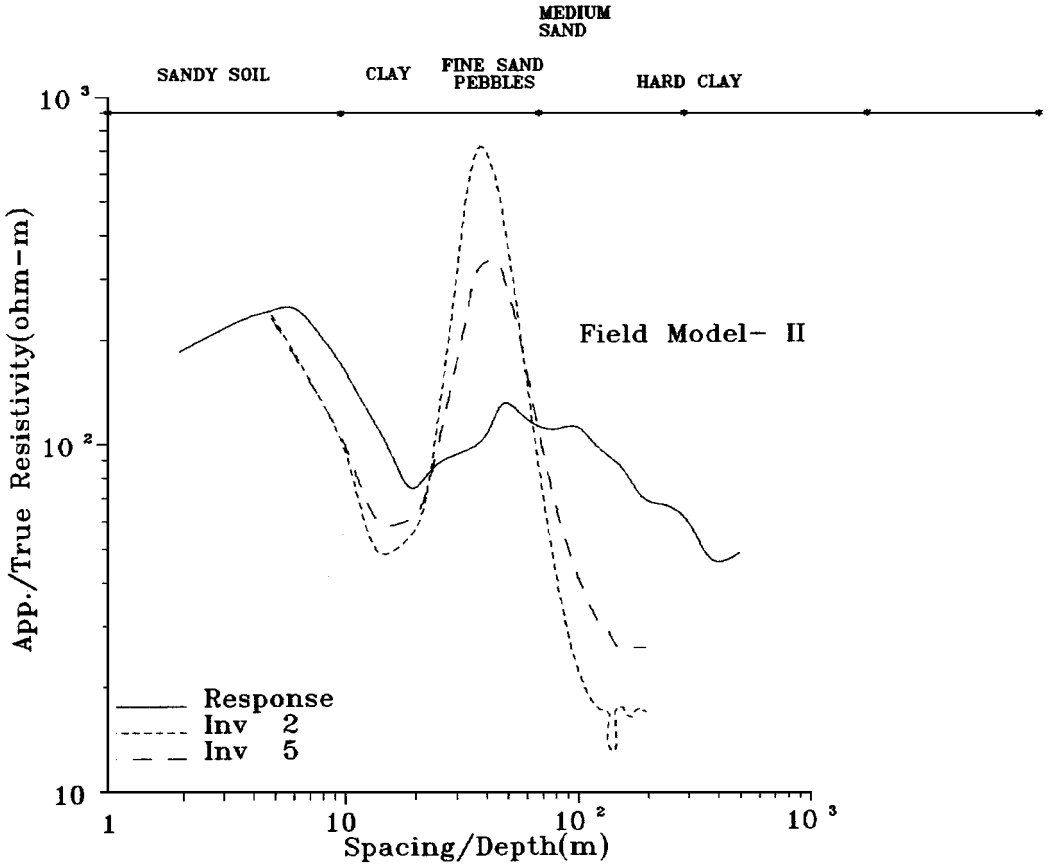

FIG. 7. The field resistivity sounding response recorded near Haridwar, India, the borehole data and the two inverted models obtained with regression parameter values 0.02 (Inv2) and 0.05 (Inv5).

CONCLUSIONS

The straightforward inversion scheme (SIS) is a powerful and efficient method for interpreting vertical electrical sounding data. As a linear scheme, SIS does not require the layer resistivities and thicknesses of the starting model. However, a layer thickness unit parameter has to be chosen judiciously, keeping in mind the resolution desired. Further, the SIS algorithm is truly noniterative, thus reducing the human interaction to a minimum. It uses the measured data directly to determine the minimum norm estimates of the coefficients T_{1j} which, in turn, are used to algebraically construct the various reflection coefficients and estimates of layer resistivities. Furthermore, unlike most other methods currently in use that require interpolation of data at appropriate values of electrode spacings, SIS has the freedom to use data as that actually measured at arbitrary electrode spacings, thereby completely eliminating this particular source of computational error.

The SIS algorithm leads to good quality solutions for a wide range of possible geological situations. Analysis of results obtained during extensive experimentation of this algorithm does, of course, bring out a number of points for caution, notably, the degeneracy of solutions that may arise from overparameterization of a geoelectric section that contains high-resistivity contrasts. But, with the benefit of such lessons, the straightforward inversion scheme, shows considerable promise of being a highly robust method for interpreting VES data.

ACKNOWLEDGMENTS

This work was supported financially by the Council of Scientific and Industrial Research, India, under the project No. 24/220/93-EMR-II. The help rendered by Ms. Anupma Rastogi and Mr. Yashpal Singh during computations is acknowledged. The authors earnestly acknowledge the positive attitudes of the editors Sven Treitel and Richard F. Sigal.

REFERENCES

Aassal, H. M., and Mahmoud, S. F., 1987, A new inversion technique for apparent resistivity measurements: IEEE Trans. Geosc. and Rem. Sens., **GE-25**, 7–10.

Bichara, M., and Lakshmanan, J., 1976, Fast automatic processing of resistivity sounding: Geophys. Prosp., **24**, 354–370.

Constable, S. E., Parker, R. L., and Constable, C. G., 1987, Occam's inversion: A practical algorithm for generating smooth models for electromagnetic sounding data: Geophysics, **52**, 289–300.

Flathe, H., 1955, A practical method of calculating geoelectrical model graphs for horizontally stratified media: Geophys. Prosp., **3**, 268–294.

Gai-Shan, Z., 1985, Asymptotic formula of the transform function for the layered earth potential and its applications to interpretation of resistivity sounding data: Geophysics, **50**, 1513–1514.

Ghosh, D. P., 1971a, The application of linear filter theory to the direct interpretation of geoelectrical resistivity sounding measurements: Geophys. Prosp., **19**, 192–217.

———1971b, Inverse filter coefficients for the computation of apparent resistivity standard curves for a horizontally stratified earth: Geophys. Prosp., **19**, 769–777.

Inman, J. R., 1975, Resistivity inversion with ridge regression: Geophysics, **40**, 798–817.

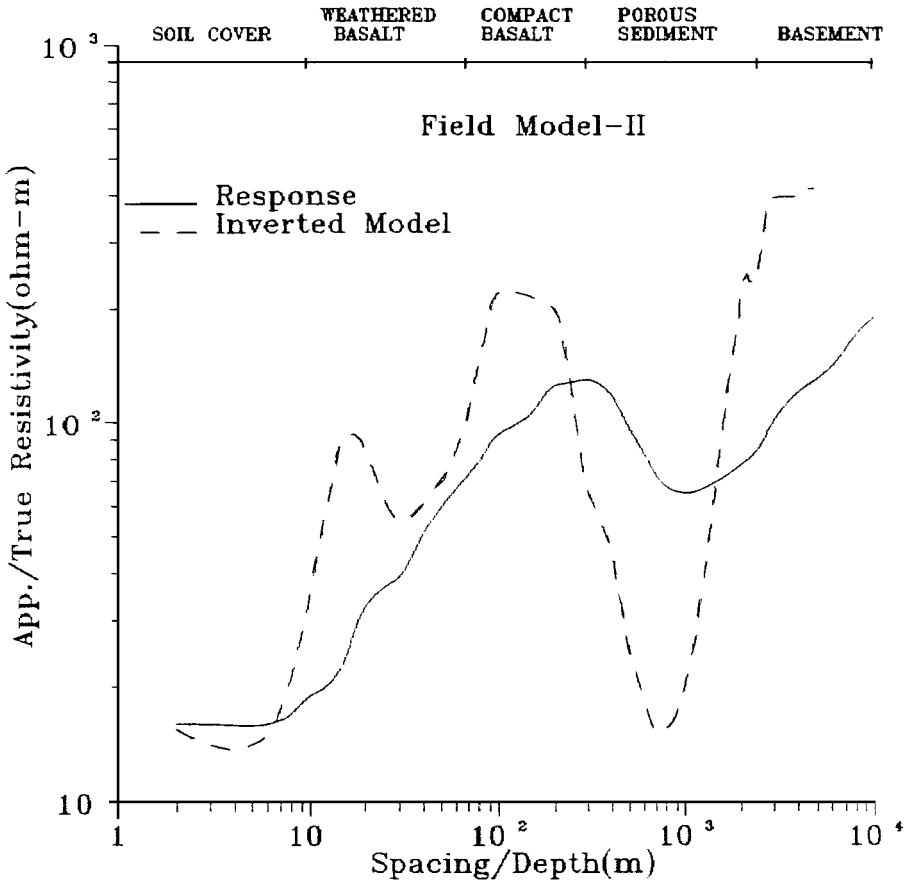

FIG. 8. The field resistivity response of a deep electrical sounding recorded in Saurashtra, India, the composite inverted model and the inferred geological section.

Inman, J. R., Ryu, J., and Ward, S. H., 1973, Resistivity inversion: Geophysics, **38**, 1088–1108.
Johansen, H. K., 1977, A man/computer interpretation system for resistivity sounding over a horizontally stratified earth: Geophys. Prosp., **25**, 667–691.
Jupp., D. L. B., and Vozoff, K., 1975, Stable iterative methods for the inversion of geophysical data: Geophys. J. Roy Astr. Soc., **42**, 957–976.
Koefoed, O., 1970, A fast method for determining the layer distribution from the raised kernel function in geoelectrical sounding: Geophys. Prosp., **18**, 564–570.
———1979, Geosounding principles 1, resistivity sounding measurements: Elsevier Science Publ. Co.
Langer, R. E., 1933, An inverse problem in differential equations: Am. Match. Soc. Bull., **39**, 814–820.
Mooney, H. M., Orellana, E., Pickett, H., and Tornheim, L., 1966, A resistivity computation method for layered earth models: Geophysics, **31**, 192–203.
Onodera, S., 1960, The kernel function in multiple layer resistivity problem: J. Geophys. Res., **65**, 3787–3794.
Parker, R. L., 1984, The inverse problem of resistivity sounding: Geophysics, **49**, 2143–2158.
Pekeris, C. L., 1940, Direct method of interpretation in resistivity prospecting: Geophysics, **5**, 31–46.
Roman, I., 1963, The kernel function in the surface potential for a horizontally stratified earth: Geophysics, **28**, 232–239.
Roy, A., and Apparao, A., 1971, Depth of investigation in direct current methods: Geophysics, **36**, 943–959.
Simms, J. E., and Morgan, F. D., 1992, Comparison of four least-squares inversionschemes for studying equivalence in one-dimensional resistivity interpretation: Geophysics, **57**, 1282–1293.
Singh, S. B., Sunder, A., Gupta, M. L., Pandey, B. P., and Das, D., 1988, Deep electrical resistivity investigations in Saurashtra Peninsula; delineation of thickness of Deccan traps and mesozoic sediments: International workshop on Deep Electromagnetic Exploration.
Slichter, L. B., 1933, The interpretation of resistivity prospecting methods for horizontal structures: Physics, **4**, 307–322.
Sri Niwas, and Israil, M., 1986, Computation of apparent resistivities using an exponential approximation of kernel function: Geophysics, **51**, 1594–1602.
———1987, A simple method of interpreting dipole resistivity sounding: Geophysics, **52**, 1412–1417.
Stefanescu, S. S., 1930, Sur la distribution electrique antour d'une prise deterre ponctuelledoms un-terrain a counha horizontales homogenes et isotropes: Le Journal de Physique et le Radium, **7**, Series 1.
Van Dam, J. C., 1964, A simple method for calculation of standard graphs to be used in geoelectrical prospecting: Ph.D. thesis, Delft Technological University.
Vozoff, K., 1958, Numerical resistivity analysis—Horizontal layers: Geophysics, **23**, 536–556.
Watson, G. N., 1958, A treatise on the theory of Bessel functions, 2nd ed., London, Cambridge Univ. Press.
Wu, Francis, T., 1968, The inverse problem of magnetotelluric sounding: Geophysics, **33**, 972–979.